Elsevier has created a Monkeypox Information Center in response to the declared public health emergency of international concern, with free information in English on the monkeypox virus. The Monkeypox Information Center is hosted on Elsevier Connect, the company's public news and information website.

Elsevier hereby grants permission to make all its monkeypox related research that is available on the Monkeypox Information Center - including this research content - immediately available in publicly funded repositories, with rights for unrestricted research re-use and analyses in any form or by any means with acknowledgement of the original source. These permissions are granted for free by Elsevier for as long as the Monkeypox Information Center remains active.

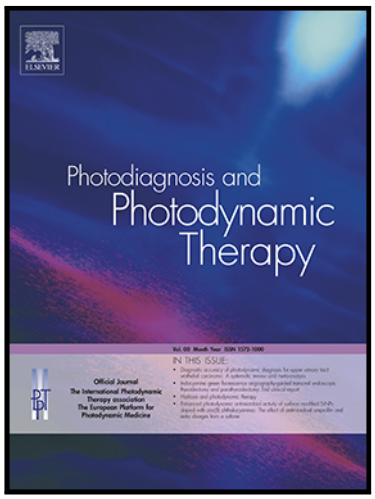

Natural photosensitizers potentiate the targeted antimicrobial photodynamic therapy as the Monkeypox virus entry inhibitors: An in silico approach

Maryam Pourhajibagher , Abbas Bahador

PII: S1572-1000(23)00383-6
DOI: https://doi.org/10.1016/j.pdpdt.2023.103656
Reference: PDPDT 103656

To appear in: *Photodiagnosis and Photodynamic Therapy*

Received date: 19 April 2023
Revised date: 13 June 2023
Accepted date: 13 June 2023

Please cite this article as: Maryam Pourhajibagher , Abbas Bahador , Natural photosensitizers potentiate the targeted antimicrobial photodynamic therapy as the Monkeypox virus entry inhibitors: An in silico approach, *Photodiagnosis and Photodynamic Therapy* (2023), doi: https://doi.org/10.1016/j.pdpdt.2023.103656

Highlights:

- Curcumin (Cur), Quercetin (Qct), and Riboflavin (Rib) as the natural photosensitizers could efficiently interact with D8L protein with a strong binding affinity.

- aPDT using Cur, Qct, and Rib may be considered an adjuvant treatment against Monkeypox disease.

- All the tested photosensitizers were found to be non-hepatotoxic and non-cytotoxic.

Natural photosensitizers potentiate the targeted antimicrobial photodynamic therapy as the Monkeypox virus entry inhibitors: An *in silico* approach

Maryam Pourhajibagher [1], Abbas Bahador [2,3*]

[1] Dental Research Center, Dentistry Research Institute, Tehran University of Medical Sciences, Tehran, Iran.
[2]Department of Microbiology, School of Medicine, Tehran University of Medical Sciences, Tehran, Iran.
[3] Fellowship in Clinical Laboratory Sciences, BioHealth Lab, Tehran, Iran.

Corresponding author:
*** Dr. Abbas Bahador**
Professor in Medical Microbiology, Department of Microbiology, Tehran University of Medical Sciences, Tehran, Iran.
E-mail: abahador@sina.tums.ac.ir

Abstract

Background: Monkeypox is a viral zoonotic disease that has emerged as a threat to public health. Currently, there is no treatment approved specifically targeting Monkeypox disease. Hence, it is essential to identify and develop therapeutic approaches to the Monkeypox virus. In the current *in silico* paper, we comprehensively involve using computer simulations and modeling to insights and predict hypotheses on the potential of natural photosensitizers-mediated targeted antimicrobial photodynamic therapy (aPDT) against D8L as a Monkeypox virus protein involved in viral cell entry.

Materials and methods: In the current study, computational techniques such as molecular docking were combined with in silico ADMET predictions to examine how Curcumin (Cur), Quercetin (Qct), and Riboflavin (Rib) as the natural photosensitizers bind to the D8L protein in Monkeypox virus, as well as to determine pharmacokinetic properties of these photosensitizers.

Results: The three-dimensional structure of the D8L protein in the Monkeypox virus was constructed using homology modeling (PDB ID: 4E9O). According to the physicochemical properties and functional characterization, 4E9O was a stable protein with the nature of a hydrophilic structure. The docking studies employing a three-dimensional model of 4E9O with

natural photosensitizers exhibited good binding affinity. D8L protein illustrated the best docking score (-7.6 kcal/mol) in relation to the Rib and displayed good docking scores in relation to the Cur (-7.0 kcal/mol) and Qct (- 7.5 kcal/mol).

Conclusions: The findings revealed that all three photosensitizers were found to obey the criteria of Lipinski's rule of five and displayed drug-likeness. Moreover, all the tested photosensitizers were found to be non-hepatotoxic and non-cytotoxic. In summary, our investigation identified Cur, Qct, and Rib could efficiently interact with D8L protein with a strong binding affinity. It can be concluded that aPDT using these natural photosensitizers may be considered an adjuvant treatment against Monkeypox disease.

Keywords: Antimicrobial photodynamic therapy, *In silico*, Monkeypox, Molecular docking

1 Introduction

Monkeypox virus as an enveloped double-stranded DNA virus belongs to the Orthopoxvirus genus in the family Poxviridae [1]. Monkeypox is typically a zoonotic disease that can not only be spread from animals to humans but human-to-human transmission occurs also via respiratory droplets, direct contact with bodily fluids of an infected person, and/or through viral particle-contaminated objects [2]. Monkeypox is a rare viral disease that often appears as a mild to moderate disease and most patients recover within 4 weeks, but it can also turn into a rapidly fatal disease.

After entering the body, Monkeypox virus begins the process of infecting cells through a complex set of interactions between viral and cellular proteins. One of the key viral proteins involved in this process is the D8L protein, which attaches to the cell surface receptor chondroitin sulfate. This binding enables the virus to enter the cell through either membrane fusion or endocytosis. Once inside the cell, the virus can replicate and spread to other parts of the body through the bloodstream, infecting a variety of tissues along the way [3].

The initial symptoms of the Monkeypox virus often initiate with fever and chills, enlarged lymph nodes (neck, armpit, and groin), severe headache, body pain, swelling of lymph nodes, fatigue, and sometimes sore throat and cough, and within one to three days after from the beginning of the fever and skin rashes appear. Rashes often appear on the face, trunk, extremities, and other areas including the genitalia [4].

The use of *in silico* computational approaches associated with bioinformatics, chemoinformatics, and molecular docking in the construction of effective drugs against diverse microorganisms has considerably increased as the first aspect of the domain of drug design, development, and discovery [5]. *In silico* methods not only can make fast predictions for a large set of compounds but also make their prediction based on the structure of a compound, even before synthesis. *In*

silico methods predict the toxicity of different compounds through quantitative structure-activity relationship (QSAR) and algorithms with toxicity data. Furthermore, *in silico* trials reduce the need for animal models and decrease the time and cost of studies [6].

According to previous studies, natural products have played a main role in drug discovery, especially for infectious diseases [7-9]. Lawson et al. showed that the higher rigidity of natural products can be effective in drug discovery by tackling protein-protein interactions [10]. Also, Doak et al. revealed that natural products are a major source of oral drugs 'beyond Lipinski's rule of five [11]. Recently, photosensitizing agents with natural origin used in the process of antimicrobial photodynamic therapy (aPDT) against various pathogens [12-15], but due to the limitations of use, including toxicity, all their pharmaceutical properties should be predicted before use.

As the Centers for Disease Control and Prevention (CDC) reported, there are no treatments specifically for Monkeypox. Hence, researchers are currently trying to find a promising approach to combat the Monkeypox virus [16]. aPDT can be an efficient approach to dealing with the Monkeypox virus. The use of aPDT, which combines light and a photosensitizing substance to kill microorganisms, is advocated as a complementary treatment for various viral infections [17-22]. Natural products have gained major interest among scientists as photosensitizers due to their unique chemical structures and properties. These compounds are found in nature and have been used for centuries in traditional medicine for their therapeutic properties. They are often biocompatible, biodegradable, and have low toxicity, making them attractive candidates for medical applications. Moreover, natural products offer a wide range of structural diversity, allowing for the discovery of new photosensitizers with unique properties. Many of these compounds are also readily available from natural sources, which can reduce the cost of production compared to synthetic photosensitizers. Curcumin (Cur), Quercetin (Qct), and Riboflavin (Rib) are natural compounds that have gained attention as potential photosensitizers for use in aPDT [23-26].

Numerous studies support the antiviral properties of these natural photosensitizers in both *in vitro* and *in vivo* investigations due to their promising antiviral effects in inhibiting polymerases, reverse transcriptase, proteases, suppressing DNA gyrase, and binding viral capsid proteins [27-30]. Rib has high quantum yields for triplet formation (0.375±0.05 in aqueous solution at pH=7) [31]. Cur has lower quantum yields for triplet formation, with values reported in the range of 0.03-0.12 in different solvents [32]. It is accepted that a longer triplet excited-state lifetime ($>10^{-6}$ s) is beneficial for aPDT, and photosensitizers showing long triplet excited-state lifetimes were used for aPDT studies [25,33]. It is important to note that the triplet quantum yield can be affected by various factors, such as the solvent, temperature, and the presence of other molecules.

There have been several studies investigating the triplet lifetimes of Cur and Rib are wide-ranging, spanning 1.8 to 10.8 μs and 13 to 120 μs, respectively, likely a result of diverse solution characteristics (e.g., pH, solvent) [34-36]. The singlet excited state lifetimes at pH 7.2 are 0.15-0.37 ns and 4.9 ± 0.1 ns for Cur and Rib, respectively [32,36]. The absorption spectrum of Cur

is a broad band with a maximum absorbance peak at a wavelength of ~425 (320-500 nm). Rib has four peaks centered in the UV at 220, 265, and 375 nm, and in visible light at 446 nm. This means that irradiation using any of these wavelengths leads to the excitation of Rib." [37,38]. Photosensitization of Cur and Rib involves the generation of reactive oxygen species (ROS), principally by the production of singlet oxygen, a central intermediate for microbiocidal action in aPDT. four peaks centered

In 2014, a research group described the photosensitizing effect of flavonols (Qct) on aPDT of the larynx (Hep-2) cancer cells [35]. However, in the UV–visible range of 240-500 nm, Qct has two main absorption bands: band A (240-280 nm) and band B (340-440 nm). The spectra are pH dependent reflecting its ionization state [39]. Cur and Qct generate a substantial quantity of singlet oxygen primarily through the type II mechanism, whereas Rib, which mainly reacts through the type I mechanism, promotes the creation of smaller amounts of singlet oxygen [40].

It is important to identify the viral-relevant molecular targets with appropriate sensitivity to aPDT. As the previous studies revealed [41-43], the computational deep learning approaches are an integral part of the drug discovery pipeline which can be used to develop candidate drugs [44]. The hypothesis of the current *in silico* approach as a scientific method involves using computer simulations and modeling to insights and predict the potential of natural photosensitizers-mediated targeted aPDT against D8L as a Monkeypox virus protein involved in viral cell entry.

2 Materials and methods

2.1. Retrieval and molecular modeling of D8L protein

The crystal structure of the selected D8L protein (PDB ID: 4E9O) was retrieved from RCSB Protein Data Bank (PDB). The physicochemical properties and functional characterization of predicted protein such as protein molecular weight, extinction coefficient (EC-quantitative study of protein-protein and protein-ligand interactions), isoelectric point (pI), instability index (II-stability of protein), aliphatic index (AI-relative volume of protein occupied by aliphatic side chains), grand average of hydropathicities (GRAVY), and amino acid composition were predicted using the ProtParam ExPASy tool. The helices, sheets, and turns of amino acid sequences related to the secondary structure of D8L were predicted by SOPMA-based secondary structure prediction. The authenticity of the predicted protein was evaluated by Ramachandran scores using the PROCHECK server, and the quality of the model structure was validated using ERRAT, Verify3D, and ProSA-web servers. Moreover, the QMEAN scoring function was calculated using SWISS-MODEL to estimate the local and the global model quality based on the geometry, the interactions, and the solvent potential of the protein model.

2.2. Prediction of the active site

The Computed Atlas of Surface Topography of proteins (CASTp) 3.0 was used to predict probable binding pockets, surface structural pockets, area, shape, and volume of every pocket and internal cavities of the selected protein.

2.3. Molecular dynamics simulation

The molecular dynamics simulation of the D8L protein was predicted by iMOD server. The iMOD server evaluated the protein stability by its main-chain deformability plot, eigenvalue, covariance map, and elastic network model.

2.4. Collection of ligands

Three natural photosensitizers as the ligands were selected for this study; these are 1: (1E,6E)-1,7-bis(4-hydroxy-3-methoxyphenyl)hepta-1,6-diene-3,5-dione (Cur), 2: 2-(3,4-dihydroxyphenyl)-3,5,7-trihydroxychromen-4-one (Qct), and 3: 7,8-dimethyl-10-[(2S,3S,4R)-2,3,4,5-tetrahydroxypentyl]benzo[g]pteridine-2,4-dione (Rib). The SDF structure of these compounds was retrieved from the DrugBank and PubChem databases.

2.5. Molecular docking

In order to perform docking, the three-dimensional X-ray crystal structure of D8L protein (PDB ID: 4E9O, resolution = 1.42Å) in complex with known inhibitors (natural photosensitizer including Cur, Qct, and Rib) was retrieved from RCSB PDB. Water molecules and other heteroatoms such as phosphate molecules were removed from the protein file and docking was conducted on CB-Dock2 server. The best binding energy was selected for evaluation, and the analysis was done based on the potential intermolecular interactions between protein and ligands.

2.6. Prediction of ADMET by computational analysis

In silico ADMET studies were performed using the ADMET predictor v.9.5 (Simulations Plus, Inc., Lancaster, CA, USA). The natural compounds were filtered for their drug-likeness properties such as the number of hydrogen bond donors, the number of hydrogen bond acceptors, and AlogP values using Lipinski's rule of five [45]. SwissADME and admetSAR programs were used to determine the pharmacokinetics properties such as absorption, distribution, metabolism, excretion, and toxicity (ADMET) profiling of compounds. Also, the toxic properties of those final compounds such as LD50 values in mg/kg, toxicity class, acute inhalation toxicity, acute oral toxicity, acute dermal toxicity, eye irritation and corrosion, skin sensitization, skin irritation, and corrosion were predicted using ProTox-II to check and verify minor toxic drugs for human use.

3 Results

3.1. Physicochemical properties and functional characterization

As mentioned previously, 4E9O was utilized as a template model for the prediction of D8L protein. Basic information revealed that it had 269 amino acids with a molecular weight of 31277.20 Da. The pI was predicted 6.76, suggesting that D8L protein is acidic. The number of positively (Arg + Lys) and negatively (Asp + Glu) charged residues of 4E9O were 28 and 30, respectively. The aliphatic index was 86.99, indicating that this protein is thermally stable and contains a high amount of hydrophobic amino acids. Moreover, the results of the ProtParam

ExPASy tool showed that the extinction coefficient of 4E9O in water at 280 nm was found to be 28545 M^{-1} cm^{-1}. Also, the instability index was computed to be 39.97, indicating the stability of this protein. The GRAVY was -0.553 and the negative GRAVY values suggest that this protein will have a good interaction with water.

3.2. Model evaluation

Results showed that 4E9O had 45.72% (123 residues) random coil, 26.39% (71 residues) extended strand, 20.45% (55 residues) alpha helix, and 7.43% (20 residues) beta turn. According to the results, the 4E9O showed the predominant nature of random coil. The protein modeling for D8L protein was performed (Figure 1). As seen in Figure 1a, 4E9O consists of 1 chain and 12 Iodide ions. The crystal structure of D8L protein (PDB ID: 4E9O) was the template lead obtained with 93.89% sequence coverage with a QMEAN value of 0.85 ± 0.05. The QMEAN values are between 0 and 1, and the higher number, the higher reliability of the predicted structure.

The validation of the three-dimensional models was confirmed by several methods. The Ramachandran plot analysis showed that 89.3% of residues fall in the most favored region and 10.7% of residues were present in the additional allowed region (Figure 1b). An overall quality factor of 89.6396 by ERRAT verified the model as good quality (Figure 1c). Quality assessment of the homology-predicted structure was made by the ProSA-web algorithm, according to which the final structure obtained a Z-score of -7.87 (Figure 1d). Also, VERIFY3D showed that 98.26% of residues had averaged 3D-1D score >= 0.2 and at least 80% of the amino acids had scored >= 0.2 in the 3D/1D profile (Figure 1e). Hence, the results display that the modeled structure of Monkeypox virus D8L protein is reasonable and reliable as a target for natural photosensitizers.

3.3. Active site prediction

According to the results in Figure 2, there are 51 amino acids in active site of 4E9O. The best pockets showed an area and volume of 231.312 (SA) $Å^2$ and 141.329 (SA) $Å^3$. The residue ASN175 located in the active site of the D8L protein plays a crucial role in the binding of the virus to host cells.

3.4. Molecular dynamics simulation

The normal mode analysis (NMA) of the protein in internal coordinates was evaluated by the iMODS server. The NMA mobility of 4E9O is shown in Figure 3a. The main-chain deformability is shown in Figure 3b. The chain 'hinges' locations are regions with high deformability. Figure 3c shows the eigenvalues which are closely related to the energy required to deform the protein structure and the eigenvalue of 4E9O is 8.848137e−04. Quantification of the uncertainty of each atom was calculated by B-factor values (Figure 3d). Figure 3e shows the variance plot. The variance plot demonstrates individual and cumulative variances in red and green color, respectively. Also, the covariance matrix between the pairs of residues is presented

in Figure 3f, indicating their correlations. The elastic network model in Figure 3g showed the connection between atoms and springs. Finally, the findings of molecular dynamic simulation results suggest that our predicted model is stable.

3.5. Molecular docking

The best orientation of the ligand was selected based on the binding interactions and docking score. The docking scores of the best-docked conformation of Cur, Qct, and Rib were -7.0, -7.5, and -7.6 kcal/mol, respectively. Figure 4 shows the binding relationship between natural photosensitizers and amino acid residues of D8L. As Figure 4a shows, Rib entered deep inside the active site of D8L and formed interactions with the amino acids residues, including LEU24 ASP25 ILE26 HIS27 TYR28 ASN29 ASP157 ASN158 LEU160 LEU164 ASN175. Cur was well fitted into the active pocket of D8L, and its hydroxyl groups formed hydrogen bonds with ILE8 ASN9 GLU11 LYS13 VAL84 ASN175 PRO222 TYR223 LYS224 LEU225 (Figure 4b). Moreover, Qct mainly interacted with D8L bridged with amino acid residues (GLN3 GLU105 GLU106 LYS108 LYS109 HIS110 ASP111 ASN175 SER177 ALA178 ASP179; Figure 4c).

3.6. ADME analysis

The ADME features of the natural photosensitizers (Cur, Qct, and Rib) including physicochemical parameters, lipophilicity, water solubility, and medicinal chemistry properties are presented in Table 1. According to the results in Table 2, all the natural photosensitizers not only displayed drug-likeness with no violation of Lipinski's rule of five but also exhibited a bioavailability score of 0.55. Moreover, the results of the pharmacokinetic properties of the natural photosensitizers such as absorption, distribution, metabolism, and excretion (ADME) are listed in Table 3. According to the skin permeation value, all ligands were predicted to be absorbed by the skin. Two of these photosensitizers, Cur and Qct, were predicted to be well absorbed from the GI tract. All ligands do not cross the BBB and are not the P-gp substrate. Cur inhibits CYP2C9 and CYP3A4 whereas CYP1A2, CYP2D6, and CYP3A4 are inhibited by Qct. By contrast, Rib does not act as an inhibitor for CYP1A2, CYP2C19, CYP2C9, CYP2D6, and CYP3A4.

3.7. Toxic properties

The *in silico* toxicity properties of the natural photosensitizers were evaluated by Pro-Tox II (Table 4). The predicted LD50 (mg/kg) for Qct, Cur, and Rib were 159, 2000, and 10000, respectively; hence, were categorized as toxicity class-3, class-4, and class-6, respectively. According to the results of Table 4, all the tested photosensitizers were found to be non-hepatotoxic and non-cytotoxic. Further, the carcinogenicity and mutagenicity of Cur and Rib were inactive in comparison with Qct.

4 Discussion

First, we selected the United States Food and Drug Administration (US FDA) approved drugs for aPDT process. As previously reported, aPDT is a new strategy to combat infections [46]. aPDT relies on the generation of ROS, via the excitation of a photosensitizer by visible light in the presence of oxygen, so that target microorganisms can be destroyed, without damaging the surrounding tissue [33]. There are several natural compounds extracted from plants and other organisms which act as a photosensitizer [48-50]. Cur, Qct, and Rib were used as the natural photosensitizing agents in the current *in silico* study. Cur derived from the rhizome of the *Curcuma longa* plant has a broad spectrum of biological functions. According to the literature, Cur exerts antiviral activities against diverse viruses such as the Influenza virus, Adenovirus, Hepatitis virus, Zikavirus, Human immunodeficiency virus (HIV), and severe acute respiratory syndrome coronavirus-2 (SARS-CoV-2) [51-53]. Qct classified as a flavonoid compound has been noted due to its tremendous pharmaceutical features including antibacterial activity, anti-inflammatory, antiplatelets, antihypertensive, antitumor, natural antihistamine, and hepatoprotective [54,55]. Moreover, early *in vitro* studies demonstrated that Qct has a dose-dependent antiviral activity against herpes simplex virus, HSV-1, and HSV-2 [56,57]. Qct can also use against the major human viruses belonging to families of Coronaviridae, Filoviridae, Flaviviridae, Hepadnaviridae, Herpesviridae, Orthomyxoviridae, Picornaviridae, Pneumoviridae, and Retroviridae [55]. Rib has been introduced as another natural, potent photosensitizing molecule that was used in the inactivation of several viruses including vesicular stomatitis virus (VSV), herpes simplex virus (HSV), SARS-CoV-2, and poliovirus in platelets was reported [58-61].

Second, the three-dimensional X-ray crystal structure of the D8L protein in the Monkeypox virus was constructed using homology modeling (PDB ID: 4E9O). Third, to evaluate the stability of the modeled protein structure, the physicochemical properties and functional characterization were assessed using the ProtParam ExPASy tool. According to the findings, 4E9O was a stable protein with the nature of the hydrophilic structure (GRAVY value=-0.553) that can interact strongly with water molecules. According to the secondary structure analysis, 4E9O was found to have a random coil, extended strand, alpha helix, and beta turn structures, with the predominant nature of a random coil.

Although the three-dimensional structure of the predicted protein displayed the desirable properties of the Ramachandran plot prediction model, the detection of errors in experimental and theoretical models of protein structures is one of the difficult problems in structural biology [62]. As a result, the ERRAT, Verify3D, and ProSA-web servers were used to predict the possible structural, modeling errors, as well as confirm the quality of the modeled structure in 4E9O. ERRAT and Verify3D verified the model as good quality. As the results of ProSA-web showed, this predicted protein got a Z-score of -7.87, suggesting the appropriateness of the model as a target for natural photosensitizers.

Fourth, the molecular docking method was used to select the ligands having the best residue interaction with the target protein. In this study, ligand-based interaction with the domains of the Monkeypox virus D8L protein was investigated using CB-Dock2 as an accurate protein-ligand

blind docking tool [63]. The binding energy values observed for Cur, Qct, and Rib were nearly equal for D8L protein; indicating all these natural photosensitizing agents interacted with D8L protein and probably have significance as the Monkeypox virus entry inhibitors.

Despite the limited understanding of the involvement of water in the binding process, it is probable that the existence of water molecules affects the interaction between the protein and ligand. While water molecules can enhance the binding affinity of ligand to the protein by stabilizing the complex, they can also compete with the ligand for binding or disrupt the hydrophobic interactions between the protein and the ligand. The conformational changes induced by the water-mediated network of hydrogen bonds can also affect the binding affinity and specificity of the complex [64-66]. Therefore, a comprehensive understanding of the role of water molecules in the D8L-Cur, D8L-Qc, and D8L-Rib interactions are crucial for the development of effective antiviral therapies targeting Monkeypox virus. The extinction coefficient of a protein in water at 280 nm is a measure of how much it absorbs light at that wavelength, and it is often used to quantify the protein concentration in a sample [67]. The acceptable range for the extinction coefficient of a protein in water at 280 nm depends on several factors, such as the specific amino acid sequence and the presence of other chromophores in the sample. However, it is important to note that this range is not absolute, and the actual value can vary depending on the protein's specific characteristics and the experimental conditions used to measure it [67,68].

Since the selection of suitable candidates with sufficient information regarding absorption, distribution, metabolism, excretion, and toxicity (ADMET) is required during the initial phase of drug discovery [69], the drug-likeness and pharmacokinetics properties of natural photosensitizers were predicted by SwissADME and admetSAR programs in the fourth phase of the current study. The results revealed the studied natural photosensitizers obeyed Lipinski’s rule of five and are likely to be good candidates in this investigation.

Since Rib, Cur, and Qct are natural photosensitizers used in aPDT as an adjunctive therapeutic strategy against infectious diseases, they may interact and interfere with other co-administered drugs during drug metabolism by inhibiting drug-metabolizing enzymes, leading to therapeutic failure or unwanted adverse effects. Therefore, it is necessary to evaluate the inhibitory effects of these natural photosensitizers on the principal members of the cytochrome P450 mixed-function oxidase system, including CYP1A2, CYP2C19, CYP2C9, CYP2D6, and CYP3A4 which are monooxygenases that catalyze many reactions involved in drug metabolism and the synthesis of cholesterol, steroids, and other lipid components. The SwissADME web tool offers access to a pool of fast, yet robust predictive models for assessing the inhibitory effects of agents on the principal members of the cytochrome P450 mixed-function oxidase system mentioned. The results of this study revealed that Rib doesn't serve as an inhibitor for the enzymes CYP1A2, CYP2C19, CYP2C9, CYP2D6, and CYP3A4. However, Cur has the ability to inhibit CYP2C9 and CYP3A4, whereas CYP1A2, CYP2D6, and CYP3A4 can be inhibited by Qct.

Eventually, the natural photosensitizers were tested for toxicity using ProTox-II. According to the globally harmonized system of classification of labeling of chemicals (GHS), six toxicity

classes were introduced as Class 1: LD50 ≤ 5 (death if swallowed), Class 2: 5 < LD50 ≤ 50 (fatal if swallowed), Class 3: 50 < LD50 ≤ 300 (toxic if swallowed), Class 4: 300 < LD50 ≤ 2000 (harmful if swallowed), Class 5: 2000 < LD50 ≤ 5000 (may be harmful if swallowed), and Class 6: LD50 > 5000 (non-toxic). The predicted LD50 (mg/kg) for the three photosensitizers ranged from 159 to 10000; Qct was categorized as toxicity class-3, indicating that this photosensitizer might be toxic if swallowed. Cur was categorized as toxicity class-4, it might be harmful if swallowed, whiles Rib with toxicity class-6 is non-toxic if swallowed.

Overall, we hope that the results of this *in silico* study might be a valuable contribution to the researchers to conduct extensive examinations on the design and manufacture of drugs and/or vaccines against the Monkeypox disease. Since the true efficacy of the natural photosensitizers could not be solely demonstrated based on *in silico* studies, *in vitro* and *in vivo* studies were recommended for the experimental validation of the findings.

Conclusion

With well-known pharmacokinetic and ADMET properties, Cur, Qct, and Rib can be considered good natural photosensitizers for further optimization and development for Monkeypox treatment. Furthermore, the results of molecular docking confirm that aPDT could be a promising adjuvant therapeutic approach against the Monkeypox virus since Cur, Qct, and Rib appear to be capable of binding to the virus's D8L protein in the early stages and can affect the binding of the D8L protein to host cell surface receptors. The residue ASN175 located in the active site of the D8L protein plays a crucial role in the binding of the virus to host cells.

Ethics approval and consent to participate

All methods were carried out in accordance with relevant guidelines and regulations.

Consent for publication

Not applicable.

Availability of data and materials

We obtained the protein sequence of D8L from NCBI database (https://www.ncbi.nlm. nih.gov). The SDF structure of Curcumin, Quercetin, and Riboflavin were retrieved from the DrugBank (https://go.drugbank.com/) and PubChem databases (https://pubchem.ncbi.nlm.nih.gov). All datasets supporting the conclusions of this article are included within the article.

Competing interests

There is no competing interest.

Funding

Not applicable.

Acknowledgements

Not applicable.

Additional information

Correspondence and requests for materials should be addressed to AB.

References

[1] Xiang Y, White A. Monkeypox virus emerges from the shadow of its more infamous cousin: family biology matters. Emerg Microbes Infect. 2022 Dec;11(1):1768-1777. doi: 10.1080/22221751.2022.2095309.

[2] Ligon BL. Monkeypox: a review of the history and emergence in the Western hemisphere. Semin Pediatr Infect Dis. 2004 Oct;15(4):280-7. doi: 10.1053/j.spid.2004.09.001.

[3] Altayb HN. Fludarabine, a potential DNA-dependent RNA polymerase inhibitor, as a prospective drug against Monkeypox virus: A computational approach. Pharmaceuticals (Basel). 2022 Sep 9;15(9):1129. doi: 10.3390/ph15091129.

[4] Yinka-Ogunleye A, Aruna O, Dalhat M, Ogoina D, McCollum A, Disu Y, et al. Outbreak of human monkeypox in Nigeria in 2017-18: a clinical and epidemiological report. Lancet Infect Dis. 2019 Aug;19(8):872-879. doi: 10.1016/S1473-3099(19)30294-4.

[5] Lipinski CA, Lombardo F, Dominy BW, Feeney PJ. Experimental and computational approaches to estimate solubility and permeability in drug discovery and development settings. Adv Drug Deliv Rev. 2001 Mar 1;46(1-3):3-26. doi: 10.1016/s0169-409x(00)00129-0.

[6] Vogel HG, Maas J, Hock FJ, Mayer D, editors. Drug Discovery and Evaluation: Safety and Pharmacokinetic Assays. Springer, Berlin, Heidelberg. 2013. https://doi.org/10.1007/978-3-642-25240-2_55.

[7] Atanasov AG, Zotchev SB, Dirsch VM; International Natural Product Sciences Taskforce, Supuran CT. Natural products in drug discovery: advances and opportunities. Nat Rev Drug Discov. 2021 Mar;20(3):200-216. doi: 10.1038/s41573-020-00114-z.

[8] Chávez-Hernández AL, Sánchez-Cruz N, Medina-Franco JL. Fragment Library of Natural Products and Compound Databases for Drug Discovery. Biomolecules. 2020 Nov 6;10(11):1518. doi: 10.3390/biom10111518.

[9] Xu Z, Eichler B, Klausner EA, Duffy-Matzner J, Zheng W. Lead/Drug Discovery from Natural Resources. Molecules. 2022 Nov 28;27(23):8280. doi: 10.3390/molecules27238280.

[10] Lawson ADG, MacCoss M, Heer JP. Importance of Rigidity in Designing Small Molecule Drugs To Tackle Protein-Protein Interactions (PPIs) through Stabilization of Desired Conformers. J Med Chem. 2018 May 24;61(10):4283-4289. doi: 10.1021/acs.jmedchem.7b01120.

[11] Doak BC, Over B, Giordanetto F, Kihlberg J. Oral druggable space beyond the rule of 5: insights from drugs and clinical candidates. Chem Biol. 2014 Sep 18;21(9):1115-42. doi: 10.1016/j.chembiol.2014.08.013.

[12] Polat E, Kang K. Natural Photosensitizers in Antimicrobial Photodynamic Therapy. Biomedicines. 2021 May 21;9(6):584. doi: 10.3390/biomedicines9060584.

[13] Alam ST, Hwang H, Son JD, Nguyen UTT, Park JS, Kwon HC, et al. Natural photosensitizers from Tripterygium wilfordii and their antimicrobial photodynamic therapeutic effects in a Caenorhabditis elegans model. J Photochem Photobiol B. 2021 May;218:112184. doi: 10.1016/j.jphotobiol.2021.112184.

[14] Nafee N, Youssef A, El-Gowelli H, Asem H, Kandil S. Antibiotic-free nanotherapeutics: hypericin nanoparticles thereof for improved in vitro and in vivo antimicrobial photodynamic therapy and wound healing. Int J Pharm. 2013 Sep 15;454(1):249-58. doi: 10.1016/j.ijpharm.2013.06.067.

[15] Suvorov N, Pogorilyy V, Diachkova E, Vasil'ev Y, Mironov A, Grin M. Derivatives of Natural Chlorophylls as Agents for Antimicrobial Photodynamic Therapy. Int J Mol Sci. 2021 Jun 15;22(12):6392. doi: 10.3390/ijms22126392.

[16] Available online: https://www.cdc.gov/poxvirus/monkeypox/about/faq.html, (accessed on 28 September 2022).

[17] Ramires MCCH, Mattia MB, Tateno RY, Palma LF, Campos L. A combination of phototherapy modalities for extensive lip lesions in a patient with SARS-CoV-2 infection. Photodiagnosis Photodyn Ther. 2021 Mar;33:102196. doi: 10.1016/j.pdpdt.2021.102196.

[18] Teitelbaum S, Azevedo LH, Bernaola-Paredes WE. Antimicrobial Photodynamic Therapy Used as First Choice to Treat Herpes Zoster Virus Infection in Younger Patient: A Case Report. Photobiomodul Photomed Laser Surg. 2020 Apr;38(4):232-236. doi: 10.1089/photob.2019.4725.

[19] Vellappally S, Mahmoud MH, Alaqeel SM, Alotaibi RN, Almansour H, Alageel O, et al. Efficacy of antimicrobial photodynamic therapy versus antiviral therapy in the treatment of herpetic gingivostomatitis among children: Aa randomized controlled clinical trial. Photodiagnosis Photodyn Ther. 2022 Sep;39:102895. doi: 10.1016/j.pdpdt.2022.102895.

[20] da Silva FC, Rosa LP, de Jesus IM, de Oliveira Santos GP, Inada NM, Blanco KC, et al. Total mouth photodynamic therapy mediated by red LED and porphyrin in individuals with AIDS. Lasers Med Sci. 2022 Mar;37(2):1227-1234. doi: 10.1007/s10103-021-03377-z.

[21] Raffaele RM, Baldo ME, Santana GU, Siqueira JM, Palma LF, Campos L. Phototherapies for erythema multiforme secondary to viral infections: A case report of a child. Photodiagnosis Photodyn Ther. 2022 Dec;40:103094. doi: 10.1016/j.pdpdt.2022.103094.

[22] Ziganshyna S, Szczepankiewicz G, Kuehnert M, Schulze A, Liebert UG, Pietsch C, Eulenburg V, Werdehausen R. Photodynamic Inactivation of SARS-CoV-2 Infectivity and Antiviral Treatment Effects In Vitro. Viruses. 2022 Jun 14;14(6):1301. doi: 10.3390/v14061301.

[23] Kah G, Chandran R, Abrahamse H. Curcumin a Natural Phenol and Its Therapeutic Role in Cancer and Photodynamic Therapy: A Review. Pharmaceutics. 2023 Feb 14;15(2):639. doi: 10.3390/pharmaceutics15020639.

[24] Gholami L, Shahabi S, Jazaeri M, Hadilou M, Fekrazad R. Clinical applications of antimicrobial photodynamic therapy in dentistry. Front Microbiol. 2023 Jan 5;13:1020995. doi: 10.3389/fmicb.2022.1020995.

[25] Aziz B, Aziz I, Khurshid A, Raoufi E, Esfahani FN, Jalilian Z, Mozafari MR, Taghavi E, Ikram M. An Overview of Potential Natural Photosensitizers in Cancer Photodynamic Therapy. Biomedicines. 2023 Jan 16;11(1):224. doi: 10.3390/biomedicines11010224.

[26] Lee IH, Kim SH, Kang DH. Quercetin mediated antimicrobial photodynamic treatment using blue light on Escherichia coli O157:H7 and Listeria monocytogenes. Curr Res Food Sci. 2022 Dec 30;6:100428. doi: 10.1016/j.crfs.2022.100428.

[27] Cotin S, Calliste CA, Mazeron MC, Hantz S, Duroux JL, Rawlinson WD, Ploy MC, Alain S. Eight flavonoids and their potential as inhibitors of human cytomegalovirus replication. Antiviral Res. 2012 Nov;96(2):181-6. doi: 10.1016/j.antiviral.2012.09.010.

[28] Hung PY, Ho BC, Lee SY, Chang SY, Kao CL, Lee SS, Lee CN. Houttuynia cordata targets the beginning stage of herpes simplex virus infection. PLoS One. 2015 Feb 2;10(2):e0115475. doi: 10.1371/journal.pone.0115475.

[29] Granato M, Gilardini Montani MS, Zompetta C, Santarelli R, Gonnella R, Romeo MA, et al. Quercetin Interrupts the Positive Feedback Loop Between STAT3 and IL-6, Promotes Autophagy, and Reduces ROS, Preventing EBV-Driven B Cell Immortalization. Biomolecules. 2019 Sep 12;9(9):482. doi: 10.3390/biom9090482.

[30] Rizky WC, Jihwaprani MC, Mushtaq M. Protective mechanism of quercetin and its derivatives in viral-induced respiratory illnesses. Egypt J Bronchol 16, 58 (2022). https://doi.org/10.1186/s43168-022-00162-6.

[31] Holzer W, Penzkofer A, Fuhrmann M, Hegemann P. Spectroscopic characterization of flavin mononucleotide bound to the LOV1 domain of Phot1 from Chlamydomonas reinhardtii. Photochem Photobiol. 2002 May;75(5):479-87. doi: 10.1562/0031-8655(2002)075<0479:scofmb>2.0.co;2.

[32] Khopde SM, Priyadarsini KI, Palit DK, Mukherjee T. Effect of solvent on the excited-state photophysical properties of curcumin. Photochem Photobiol. 2000 Nov;72(5):625-31. doi: 10.1562/0031-8655(2000)072<0625:eosote>2.0.co;2.

[33] Takemura T, Ohta N, Nakajima S, Sakata I. Critical importance of the triplet lifetime of photosensitizer in photodynamic therapy of tumor. Photochem Photobiol. 1989 Sep;50(3):339-44. doi: 10.1111/j.1751-1097.1989.tb04167.x.

[34] Priyadarsini KI. Photophysics, photochemistry and photobiology of curcumin: Studies from organic solutions, bio-mimetics and living cells. J Photochem Photobiol C. 2009 Jun 1;10(2):81-95. doi.org/10.1016/j.jphotochemrev.2009.05.001.

[35] de Paula Rodrigues R, Tini IR, Soares CP, da Silva NS. Effect of photodynamic therapy supplemented with quercetin in HEp-2 cells. Cell Biol Int. 2014 Jun;38(6):716-22. doi: 10.1002/cbin.10251.

[36] Gutiérrez MI, Fernández SM, Massad WA, García NA. Kinetic study on the photostability of riboflavin in the presence of barbituric acid. Redox Report. 2006 Aug 1;11(4):153-8. doi: 10.1179/135100006X116655.

[37] Bartzatt R, Follis ML. Detection and assay of riboflavin (vitamin B2) utilizing UV/VIS spectrophotometer and citric acid buffer. Journal of Scientific Research and Reports. 2014;3(6):799.

[38] Scurachio RS, Mattiucci F, Santos WG, Skibsted LH, Cardoso DR. Caffeine metabolites not caffeine protect against riboflavin photosensitized oxidative damage related to skin and eye health. J Photochem Photobiol B. 2016 Oct;163:277-83. doi: 10.1016/j.jphotobiol.2016.08.042.

[39] Buchweitz M, Kroon PA, Rich GT, Wilde PJ. Quercetin solubilisation in bile salts: A comparison with sodium dodecyl sulphate. Food Chem. 2016 Nov 15;211:356-64. doi: 10.1016/j.foodchem.2016.05.034.

[40] Insińska-Rak M, Sikorski M. Riboflavin interactions with oxygen-a survey from the photochemical perspective. Chemistry. 2014 Nov 17;20(47):15280-91. doi: 10.1002/chem.201403895.

[41] Pourhajibagher M, Bahador A. Virtual screening and computational simulation analysis of antimicrobial photodynamic therapy using propolis-benzofuran A to control of Monkeypox. Photodiagnosis Photodyn Ther. 2022 Nov 20;41:103208. doi: 10.1016/j.pdpdt.2022.103208.

[42] Pourhajibagher M. Molecular Modeling and Simulation Analysis of Antimicrobial Photodynamic Therapy Potential for Control of COVID-19. Scientific World Journal. 2022 May 31;2022:7089576. doi: 10.1155/2022/7089576.

[43] Pourhajibagher M, Bahador A. Molecular docking study of potential antimicrobial photodynamic therapy as a potent inhibitor of SARS-CoV-2 main protease: An in silico insight. Infect Disord Drug Targets. 2022 Sep 1. doi: 10.2174/1871526522666220901164329.

[44] Sliwoski G, Kothiwale S, Meiler J, Lowe EW Jr. Computational methods in drug discovery. Pharmacol Rev. 2013 Dec 31;66(1):334-95. doi: 10.1124/pr.112.007336.

[45] Pinzi L, Rastelli G. Molecular Docking: Shifting Paradigms in Drug Discovery. Int J Mol Sci. 2019 Sep 4;20(18):4331. doi: 10.3390/ijms20184331.

[46] Şen Karaman D, Ercan UK, Bakay E, Topaloğlu N, Rosenholm JM. Evolving technologies and strategies for combating antibacterial resistance in the advent of the postantibiotic era. Adv Funct Mater. 2020 Apr;30(15):1908783. doi: 10.1002/adfm.201908783.

[47] Ghorbani J, Rahban D, Aghamiri S, Teymouri A, Bahador A. Photosensitizers in antibacterial photodynamic therapy: an overview. Laser Ther. 2018 Dec 31;27(4):293-302. doi: 10.5978/islsm.27_18-RA-01.

[48] Kubrak TP, Kołodziej P, Sawicki J, Mazur A, Koziorowska K, Aebisher D. Some Natural Photosensitizers and Their Medicinal Properties for Use in Photodynamic Therapy. Molecules. 2022 Feb 10;27(4):1192. doi: 10.3390/molecules27041192.

[49] Xiao Q, Wu J, Pang X, Jiang Y, Wang P, Leung AW, et al. Discovery and Development of Natural Products and their Derivatives as Photosensitizers for Photodynamic Therapy. Curr Med Chem. 2018;25(7):839-860. doi: 10.2174/0929867324666170823143137.

[50] Quinn JC, Kessell A, Weston LA. Secondary plant products causing photosensitization in grazing herbivores: their structure, activity and regulation. Int J Mol Sci. 2014 Jan 21;15(1):1441-65. doi: 10.3390/ijms15011441.

[51] Kumar Verma A, Kumar V, Singh S, Goswami BC, Camps I, Sekar A, et al. Repurposing potential of Ayurvedic medicinal plants derived active principles against SARS-CoV-2 associated target proteins revealed by molecular docking, molecular dynamics and MM-PBSA studies. Biomed Pharmacother. 2021 May;137:111356. doi: 10.1016/j.biopha.2021.111356.

[52] Ardebili A, Pouriayevali MH, Aleshikh S, Zahani M, Ajorloo M, Izanloo A, et al. Antiviral Therapeutic Potential of Curcumin: An Update. Molecules. 2021 Nov 19;26(22):6994. doi: 10.3390/molecules26226994.

[53] Pourhajibagher M, Azimi M, Haddadi-Asl V, Ahmadi H, Gholamzad M, Ghorbanpour S, et al. Robust antimicrobial photodynamic therapy with curcumin-poly (lactic-co-glycolic acid) nanoparticles against COVID-19: A preliminary in vitro study in Vero cell line as a model. Photodiagnosis Photodyn Ther. 2021 Jun;34:102286. doi: 10.1016/j.pdpdt.2021.102286.

[54] Agrawal PK, Agrawal C, Blunden G. Quercetin: Antiviral Significance and Possible COVID-19 Integrative Considerations. Nat Prod Commun. 2020;15(12). doi:10.1177/1934578X20976293.

[55] Di Petrillo A, Orrù G, Fais A, Fantini MC. Quercetin and its derivates as antiviral potentials: A comprehensive review. Phytother Res. 2022 Jan;36(1):266-278. doi: 10.1002/ptr.7309.

[56] Lyu SY, Rhim JY, Park WB. Antiherpetic activities of flavonoids against herpes simplex virus type 1 (HSV-1) and type 2 (HSV-2) in vitro. Arch Pharm Res. 2005 Nov;28(11):1293-301. doi: 10.1007/BF02978215.

[57] Lee S, Lee HH, Shin YS, Kang H, Cho H. The anti-HSV-1 effect of quercetin is dependent on the suppression of TLR-3 in Raw 264.7 cells. Arch Pharm Res. 2017 May;40(5):623-630. doi: 10.1007/s12272-017-0898-x.

[58] Yuksel N, Bilgihan K, Hondur AM. Herpetic keratitis after corneal collagen cross-linking with riboflavin and ultraviolet-A for progressive keratoconus. Int Ophthalmol. 2011 Dec;31(6):513-5. doi: 10.1007/s10792-011-9489-x.

[59] Mirshafiee H, Sharifi Z, Hosseini SM, Yari F, Nikbakht H, Latifi H. The Effects of Ultraviolet Light and Riboflavin on Inactivation of Viruses and the Quality of Platelet Concentrates at Laboratory Scale. Avicenna J Med Biotechnol. 2015 Apr-Jun;7(2):57-63.

[60] Al-Qarni A, AlHarbi M. Herpetic Keratitis after Corneal Collagen Cross-Linking with Riboflavin and Ultraviolet-A for Keratoconus. Middle East Afr J Ophthalmol. 2015 Jul-Sep;22(3):389-92. doi: 10.4103/0974-9233.159777.

[61] Keil SD, Ragan I, Yonemura S, Hartson L, Dart NK, Bowen R. Inactivation of severe acute respiratory syndrome coronavirus 2 in plasma and platelet products using a riboflavin and ultraviolet light-based photochemical treatment. Vox Sang. 2020 Aug;115(6):495-501. doi: 10.1111/vox.12937.

[62] Shantier SW, Mustafa MI, Abdelmoneim AH, Fadl HA, Elbager SG, Makhawi AM. Novel multi epitope-based vaccine against monkeypox virus: vaccinomic approach. Sci Rep. 2022 Sep 25;12(1):15983. doi: 10.1038/s41598-022-20397-z.

[63] Liu Y, Grimm M, Dai WT, Hou MC, Xiao ZX, Cao Y. CB-Dock: a web server for cavity detection-guided protein-ligand blind docking. Acta Pharmacol Sin. 2020 Jan;41(1):138-144. doi: 10.1038/s41401-019-0228-6.

[64] Ladbury JE. Just add water! The effect of water on the specificity of protein-ligand binding sites and its potential application to drug design. Chem Biol. 1996 Dec;3(12):973-80. doi: 10.1016/s1074-5521(96)90164-7.

[65] Wang L, Berne BJ, Friesner RA. Ligand binding to protein-binding pockets with wet and dry regions. Proc Natl Acad Sci U S A. 2011 Jan 25;108(4):1326-30. doi: 10.1073/pnas.1016793108. Epub 2011 Jan 4. Erratum in: Proc Natl Acad Sci U S A. 2012 Jun 5;109(23):9220.

[66] Schiebel J, Gaspari R, Wulsdorf T, Ngo K, Sohn C, Schrader TE, Cavalli A, Ostermann A, Heine A, Klebe G. Intriguing role of water in protein-ligand binding studied by neutron crystallography on trypsin complexes. Nat Commun. 2018 Sep 3;9(1):3559. doi: 10.1038/s41467-018-05769-2.

[67] Pace CN, Vajdos F, Fee L, Grimsley G, Gray T. How to measure and predict the molar absorption coefficient of a protein. Protein Sci. 1995 Nov;4(11):2411-23. doi: 10.1002/pro.5560041120.

[68] Simpson, Richard J., Adams, Peter D. , and Golemis, Erica A.; Basic Methods in Protein Purification and Analysis – A laboratory manual. CSH Press. 2009.

[69] Abishad P, Niveditha P, Unni V, Vergis J, Kurkure NV, Chaudhari S, et al. In silico molecular docking and in vitro antimicrobial efficacy of phytochemicals against multi-drug-resistant enteroaggregative Escherichia coli and non-typhoidal Salmonella spp. Gut Pathog. 2021 Jul 17;13(1):46. doi: 10.1186/s13099-021-00443-3.

Properties	Curcumin	Quercetin	Riboflavin
Physicochemical			
Number of heavy atoms	27	22	27
Number of aromatic heavy atoms	12	16	14
Fraction Csp3	0.14	0.00	0.41
Molar refractivity	102.80	78.03	96.99
Lipophilicity			
Log $Po_{/w}$ (XLOGP3)	3.20	1.54	-1.46
Log $Po_{/w}$ (WLOGP)	3.15	1.99	-1.68
Log $Po_{/w}$ (MLOGP)	1.47	-0.56	-0.54
Log $P_{o/w}$ (SILICOS-IT)	4.04	1.54	1.09
Consensus Log $P_{o/w}$	3.03	1.23	-0.32
Water solubility			
Log *S* (ESOL)	-3.94	-3.16	-1.31
Solubility	4.22e-02 mg/ml; 1.15e-04 mol/l	2.11e-01 mg/ml; 6.98e-04 mol/l	1.85e+01 mg/ml; 4.93e-02 mol/l
Class	Soluble	Soluble	Very soluble
Log *S* (Ali)	-4.83	-3.91	-1.43
Solubility	5.50e-03 mg/ml; 1.49e-05 mol/l	3.74e-02 mg/ml; 1.24e-04 mol/l	1.40e+01 mg/ml; 3.72e-02 mol/l

Class	Moderately soluble	Soluble	Very soluble
Log *S* (SILICOS-IT)	-4.45	-3.24	-2.62
Solubility	1.31e-02 mg/ml; 3.56e-05 mol/l	1.73e-01 mg/ml; 5.73e-04 mol/l	9.03e-01 mg/ml; 2.40e-03 mol/l
Class	Moderately soluble	Soluble	Soluble
Medicinal chemistry			
Leadlikeness	No	Yes	No
Synthetic accessibility	2.97	3.23	3.84

Table 1. *In silico* ADME analysis of the natural photosensitizers computed by SwissADME.

Table 2. Drug-likeness predictions of natural photosensitizers computed by SwissADME.

Drug likeness properties	Curcumin	Quercetin	Riboflavin
Formula	C21H20O6	C15H10O7	C17H20N4O6
Molecular weight	368.38 g/mol	302.24 g/mol	376.36 g/mol
Number of rotatable bonds	8	1	5
Number of H-bond acceptor	6	7	8
Number of H-bond donor	2	5	5
LogP	3.27	1.63	0.97
TPSA	93.06 Å²	131.36 Å²	161.56 Å²
Lipinski's rule of five violation	0	0	0
Bioavailability score	0.55	0.55	0.55

Table 3. Pharmacokinetic properties of natural photosensitizers.

Properties		Curcumin	Quercetin	Riboflavin
Skin permeation value (log Kp) cm/s		-6.28	-7.05	-9.63
GI absorption		High	High	Low
BBB permeant		No	No	No
P-gp substrate		No	No	No
Inhibitor	**CYP1A2**	No	Yes	No
	CYP2C19	No	No	No
	CYP2C9	Yes	No	No
	CYP2D6	No	Yes	No
	CYP3A4	Yes	Yes	No

Abbreviations: GI, gastro-intestinal; BBB, blood brain barrier; P-gp, P-glycoprotein; CYP, cytochrome-P.

Table 4. Toxicity prediction of the natural photosensitizers computed by Pro-Tox II.

Properties		Curcumin		Quercetin		Riboflavin	
		Prediction	**Probability**	**Prediction**	**Probability**	**Prediction**	**Probability**
LD50 (mg/kg)		-	2000	-	159	-	10000
Toxicity class		-	4	-	3	-	6
Organ Toxicity	**Hepatotoxicity**	Inactive	0.61	Inactive	0.69	Inactive	0.93
	Carcinogenicity	Inactive	0.84	Active	0.68	Inactive	0.75
	Immunotoxicity	Active	0.92	Inactive	0.87	Inactive	0.94
	Mutagenicity	Inactive	0.88	Active	0.51	Inactive	0.72
	Cytotoxicity	Inactive	0.88	Inactive	0.99	Inactive	0.75

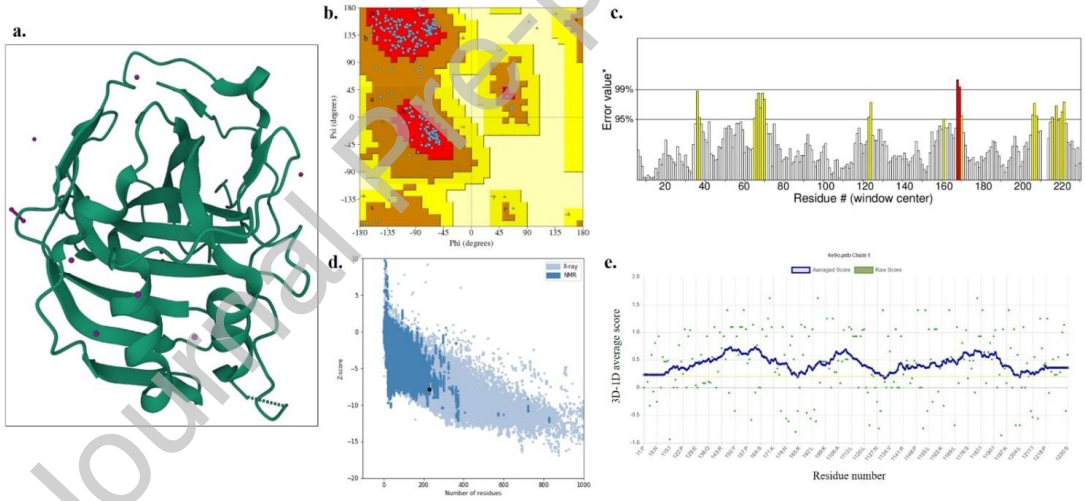

Figure 1. Structure and validation of the Monkeypox virus D8L protein-predicted structure: a. The predicted three-dimensional structure, b. Ramachandran plot, c. ERRAT, d. ProSA-web, and e. Verify3D.

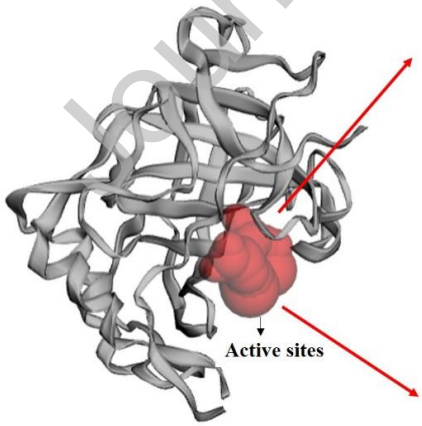

No.	Seq ID	AA	Atom	No.	Seq ID	AA	Atom	No.	Seq ID	AA	Atom	No.	Seq ID	AA	Atom
1	39	THR	CB	**14**	64	SER	OG	**27**	104	TYR	CZ	**40**	175	ASN	CA
2	39	THR	OG1	**15**	65	SER	OG	**28**	104	TYR	OH	**41**	175	ASN	CB
3	39	THR	CG2	**16**	67	HIS	ND1	**29**	108	LYS	CE	**42**	175	ASN	CG
4	41	LYS	O	**17**	67	HIS	CE1	**30**	108	LYS	NZ	**43**	175	ASN	OD1
5	41	LYS	CB	**18**	67	HIS	NE2	**31**	116	ILE	CG2	**44**	175	ASN	ND2
6	41	LYS	CG	**19**	69	TYR	CE2	**32**	116	ILE	CD1	**45**	177	SER	OG
7	41	LYS	CE	**20**	69	TYR	OH	**33**	173	THR	CB	**46**	182	TRP	CH2
8	42	LEU	CB	**21**	92	ASN	CB	**34**	173	THR	CG2	**47**	218	ASN	O
9	42	LEU	CG	**22**	92	ASN	ND2	**35**	174	ILE	N	**48**	218	ASN	CB
10	42	LEU	CD1	**23**	94	VAL	CG1	**36**	174	ILE	CB	**49**	220	ARG	CB
11	42	LEU	CD2	**24**	94	VAL	CG2	**37**	174	ILE	CG1	**50**	220	ARG	NE
12	44	ARG	CD	**25**	104	TYR	CE1	**38**	174	ILE	CG2	**51**	220	ARG	NH2
13	44	ARG	NH1	**26**	104	TYR	CE2	**39**	175	ASN	N				

Abbreviation: Seq: Sequence, AA: Amino acid.

Figure 2. Predicted active site of the Monkeypox virus D8L protein and its amino acids.

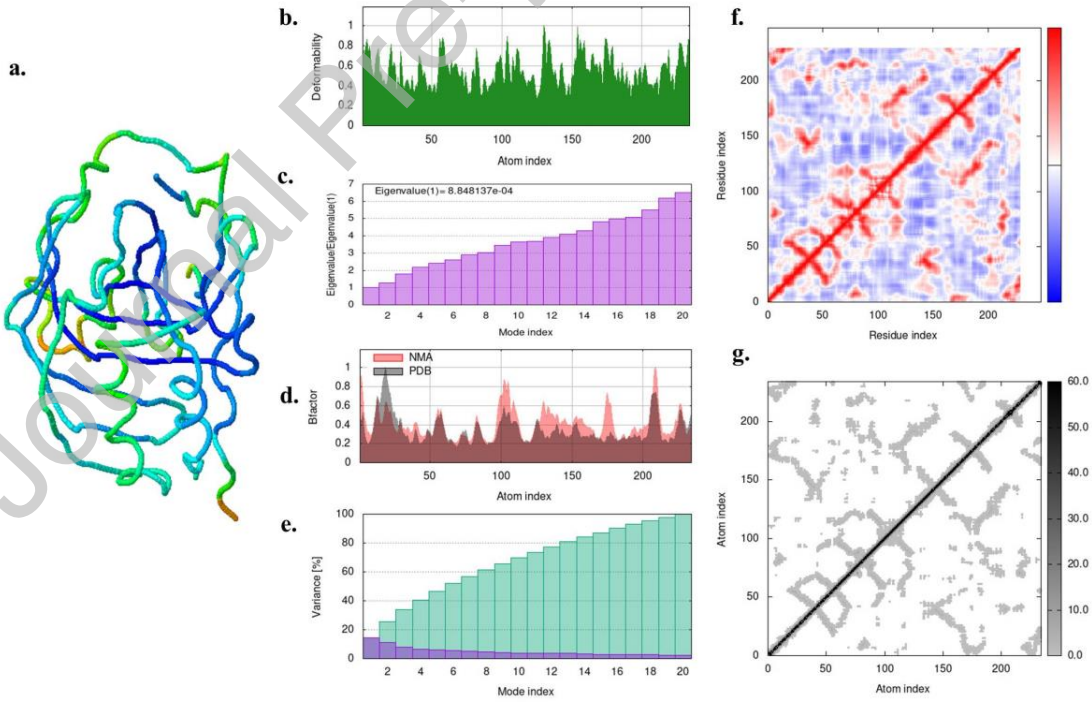

Figure 3. The molecular dynamics simulation of the Monkeypox virus D8L protein: a. NMA mobility, b. Deformability, c. Eigenvalues, d. B-factor values, e. Variance (red: individual variances, green: cumulative variances), f. Co-variance map (residues with correlated motions in red, uncorrelated motions in white, and anti-correlated motions in blue), and g) Elastic network (darker grays indicate stiffer springs).

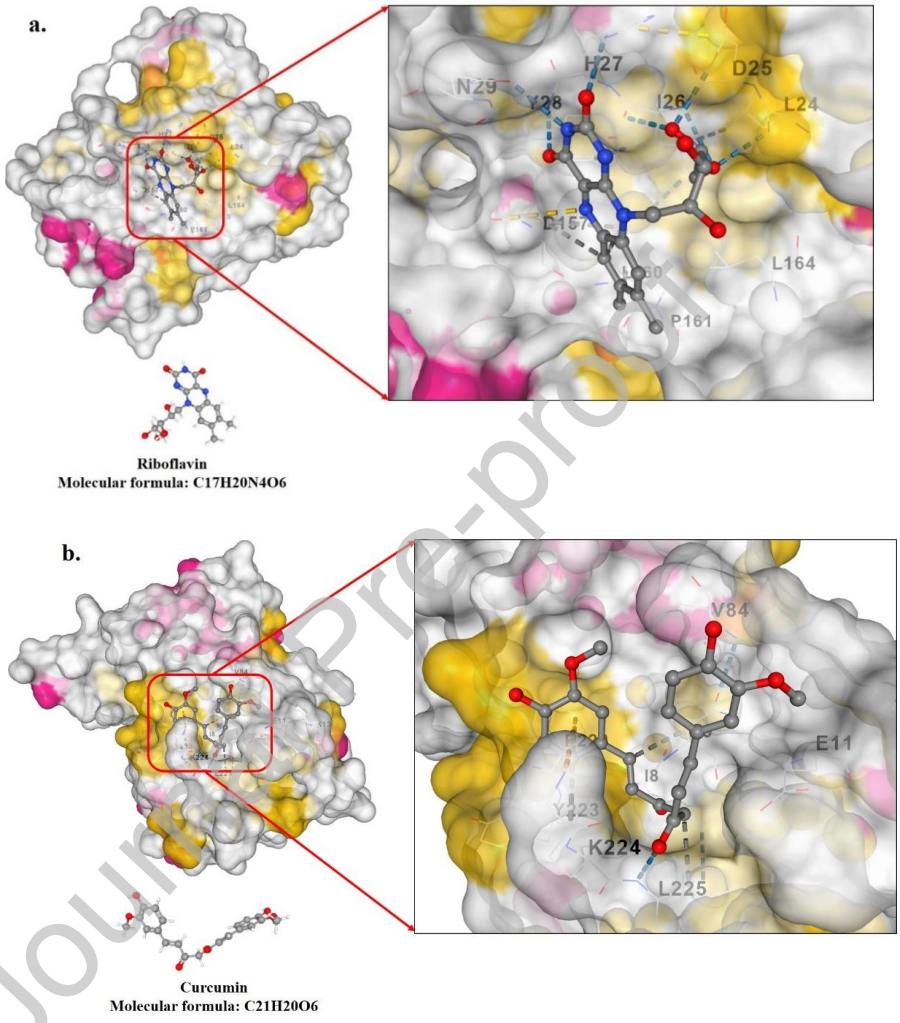

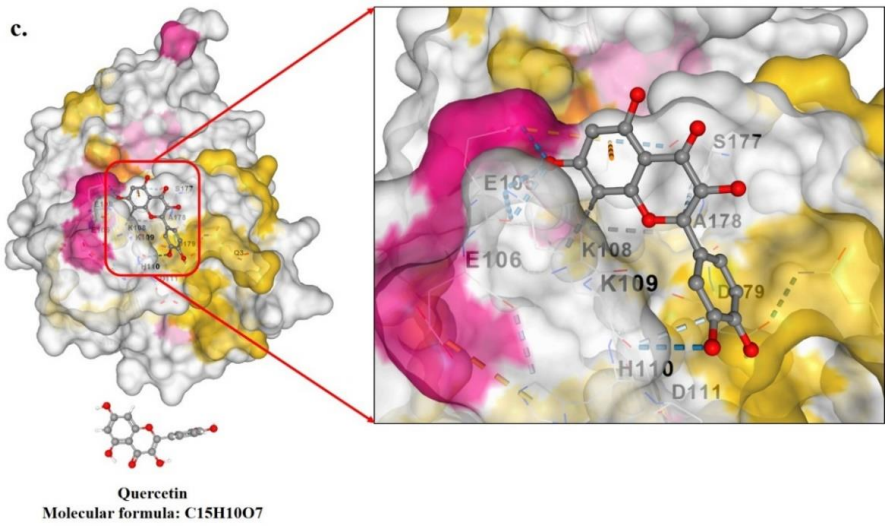

Figure 4. Representation of docked ligand-protein complex: Interaction of the amino acid residues of the Monkeypox virus D8L protein with a. Rib, b. Cur, and c. Qct.